applied sciences

IMPACT FACTOR 2.5

CITESCORE 5.3

Article

Simulation Study on Attosecond Inverse Compton Scattering Source from Laser Wakefield Acceleration with Near-Threshold Ionization Injection

Aihua Deng, Yan Li, Yugan Weng, Zhiling Luo, Xitao Yu and Jiaolong Zeng

MDPI

https://doi.org/10.3390/app14177749

applied sciences

MDPI

Article

Simulation Study on Attosecond Inverse Compton Scattering Source from Laser Wakefield Acceleration with Near-Threshold Ionization Injection

Aihua Deng [1,*], Yan Li [1], Yugan Weng [1], Zhiling Luo [1], Xitao Yu [1] and Jiaolong Zeng [1,2]

[1] School of Physics, Zhejiang University of Technology, Hangzhou 310023, China; 211122090058@zjut.edu.cn (Y.L.); 202003170321@zjut.edu.cn (Y.W.); 2112109044@zjut.edu.cn (Z.L.); yuxitao@zjut.edu.cn (X.Y.); jlzeng@zjut.edu.cn (J.Z.)

[2] Department of Physics, College of Liberal Arts and Sciences, National University of Defense Technology, Changsha 410073, China

* Correspondence: aihuadeng@zjut.edu.cn

Abstract: We present the generation of attosecond gamma rays via inverse Compton scattering within the framework of laser wakefield acceleration through 2D Particle-In-Cell simulations. Utilizing the near-threshold ionization injection mechanism, an attosecond micro-bunched electron beam characterized by a comb-like current density profile can be achieved with a linearly polarized laser at an intensity of $a_0 = 1.5$. The micro-bunched beam provides a beam energy of approximately 300 MeV and achieves a minimum relative energy spread of about 1.64% after undergoing 2 mm of acceleration. In the inverse Compton scattering scheme, these attosecond electron micro-bunches interact with the reflected driving laser pulse, resulting in the attosecond gamma-ray radiation exhibiting similar structures. Individual spatial-separated gamma-ray pulses exhibit a length of approximately 260–300 as, with a critical energy of 2.0 ± 0.2 MeV. The separated attosecond gamma-ray source owns a peak brilliance of ~10^{22} photons s^{-1} mm^{-2} $mrad^{-2}$ 0.1% BW. This brilliance is competitive in a laboratory for multi-MeV γ-ray sources with a laser intensity of $I = 5 \times 10^{18}$ W/cm^2. Such attosecond gamma-ray radiation offers promising applications requiring ultrashort X-ray/gamma ray sources.

Keywords: attosecond gamma-ray; inverse Compton scattering; discrete phase ionization; electron micro-bunching

Citation: Deng, A.; Li, Y.; Weng, Y.; Luo, Z.; Yu, X.; Zeng, J. Simulation Study on Attosecond Inverse Compton Scattering Source from Laser Wakefield Acceleration with Near-Threshold Ionization Injection. *Appl. Sci.* **2024**, *14*, 7749. https://doi.org/10.3390/app14177749

Academic Editor: Eun Ha Choi

Received: 22 July 2024
Revised: 23 August 2024
Accepted: 30 August 2024
Published: 2 September 2024

1. Introduction

Laser-driven plasma wakefield accelerators (LWFAs) show promise as compact electron accelerators [1–3]. In LWFAs, an intense laser pulse propagates through initially neutral and homogeneous plasma. The ponderomotive force of the laser expels electrons from the high-intensity region, forming a bubble structure with an acceleration gradient exceeding 100 GV/m. Experimental evidence has demonstrated that LWFA can produce electron energies of approximately 10 GeV [4,5] over 10 cm using a petawatt laser system. Unique properties, such as kiloampere peak current [6–8], few-femtoseconds (fs) bunch length [8], low energy spread [9], and low emittance [10,11], can be further enhanced by modulating the plasma profiles or controlling the electron injection processes. These characteristics imply that the electron beam has the potential to generate X-ray/gamma-ray sources with excellent collimation, narrow bandwidth, tunability, ultra-short duration, and high peak brightness [12]. By colliding relativistic electron beams with intense laser pulses, inverse Compton scattering (ICS) can occur, producing high-energy gamma rays alongside the electrons. This method might yield brightness levels far surpassing those achieved by traditional accelerators. In the head-on ICS scheme (where laser pulse and electrons interact in the 180° direction), the duration of the resulting X-rays/gamma rays essentially matches the length of the electron beam [13]. This observation suggests a pathway for

further reducing the pulse duration of the X-ray/gamma-ray to sub-femtosecond or even attosecond scales. Compact and bright gamma-ray sources, characterized by ultra-short durations and energies up to several megaelectronvolts (MeVs), demonstrate significant potential across various applications, including ultrafast chemical and biological process diagnostics [14], as well as industrial and defense research [15].

Known as a "photon collider", ICS involves a laser photon scattering off relativistic electrons, primarily relying on the double Doppler effect to shift its energy. In the context of an ICS source driven by laser wakefield acceleration, the critical energy of the head-on ICS collision photons can be estimated as follows [12,16]:

$$E_\gamma \approx 4\gamma_e^2 \hbar\omega_L f(a_0) \quad (1)$$

with $f(a_0) \approx 1$ for $a_0 \ll 1$ and $f(a_0) \approx a_0$ for $a_0 \geq 1$, where E_γ is the gamma-ray photon energy, γ is the electron relativistic factor, a_0 is the normalized laser vector potential, and $\hbar\omega_L$ is the laser photon energy. If the scattering laser vector potential $a_0 \ll 1$, Compton scattering emissions are primarily fundamental. In the case of a head-on collision, the scattered energy observed on-axis roughly scales as $4\gamma_e^2\hbar\omega_L$. The scattering enters the nonlinear regime at higher laser intensities $a_0 \geq 1$, resulting in a radiation spectrum with higher frequencies. This nonlinear effect offers a more efficient option for generating higher-energy X-rays than the LWFA-driven Betatron radiation sources. Two configurations of experimental setup are tested to produce all-optical Compton scattering sources from LWFA electrons [16–23]. The dual-pulse approach offers flexibility by employing two independent laser pulses, although achieving spatial overlap with micron accuracy and femtosecond synchronization remains highly challenging. Alternatively, a single-laser pulse reflected by a plasma mirror presents a robust and self-synchronized approach [17,21,23], albeit accompanied by non-negligible bremsstrahlung radiation [24]. Recent experiments have demonstrated precise-tunable, narrowband, collimated X-ray beams from ICS based on LWFA [25,26], showing significant potential in various applications.

One crucial application of radiation sources based on laser-plasma interaction would be time-resolved pump-probe investigations with sub-femtosecond resolution, as the radiation concentrates within a micrometer-sized volume. Unlike Free Electron Lasers (FELs), the ICS source is typically not regarded as a diffraction-limited source due to its incoherent emission, broad angular distribution, and significant divergence. The effective characteristics of the emitted radiation, such as brilliance and pulse duration, are heavily influenced by the physical size of the source and its distance from the detector. Achieving an attosecond electron bunch would represent a major milestone, potentially enabling secondary attosecond X-ray sources and significantly advancing the study of matter on sub-femtosecond time scales.

In this work, we present the generation of an attosecond ICS source from a density-modulated electron beam in LWFA. By employing the near-threshold ionization injection with a normalized laser intensity $a_0 = 1.5$ ($I = 5 \times 10^{18}\mathrm{W/cm^2}$), we achieved an attosecond electron bunch train characterized by a comb-like current density profile after 2 mm of acceleration, yielding energies of approximately 300 MeV with energy spreads of about 0.71% for individual micro bunch through 2D PIC simulations. Subsequently, this beam scattered the reflected driving laser, transferring its characteristics to the ICS X-ray source and thereby producing ICS sources with corresponding durations. The separated gamma-ray pulses exhibit an average width of approximately 300 as, with a critical energy of 2.0 ± 0.2 MeV. In the 0.1% bandwidth around 2 MeV, the generated gamma-ray source has a peak brilliance of ~10^{22} photons $\mathrm{s^{-1}\ mm^{-2}\ mrad^{-2}}$ 0.1% BW. This brilliance is competitive in a laboratory for multi-MeV γ-ray sources with a laser intensity of $\mathrm{I} = 5 \times 10^{18}\ \mathrm{W/cm^2}$. They can enhance the temporal resolution of sampling of the ultrafast fundamental physical processes by an order of magnitude while maintaining their other advantageous features such as a small source size of several microns enabling high-resolution images and a relatively small cost of the required laser systems compared to the large-scale facilities such as synchrotrons or free electron lasers [27,28].

2. Simulation Setup

The setup for the proposed attosecond LWFA-based ICS source is shown in Figure 1a. An intense femtosecond pulse drives laser–plasma wakefield, with a near-threshold ionization injection proposed to generate a density-modulated electron bunch. Downstream of the LWFA stage, a 20 μm thick aluminum (Al) foil is positioned along the propagation axis of the driving laser pulse. The Al foil is ionized by the rising edge of the laser pulse, forming a plasma mirror that effectively reflects the pulse. This approach ensures the inherent temporal and spatial overlap between the backward-propagating pulse and relativistic electrons, which is crucial for ICS. Upon collision with the micro-bunched electron beam, the reflected laser pulse emits a train of high-energy gamma-ray pulses.

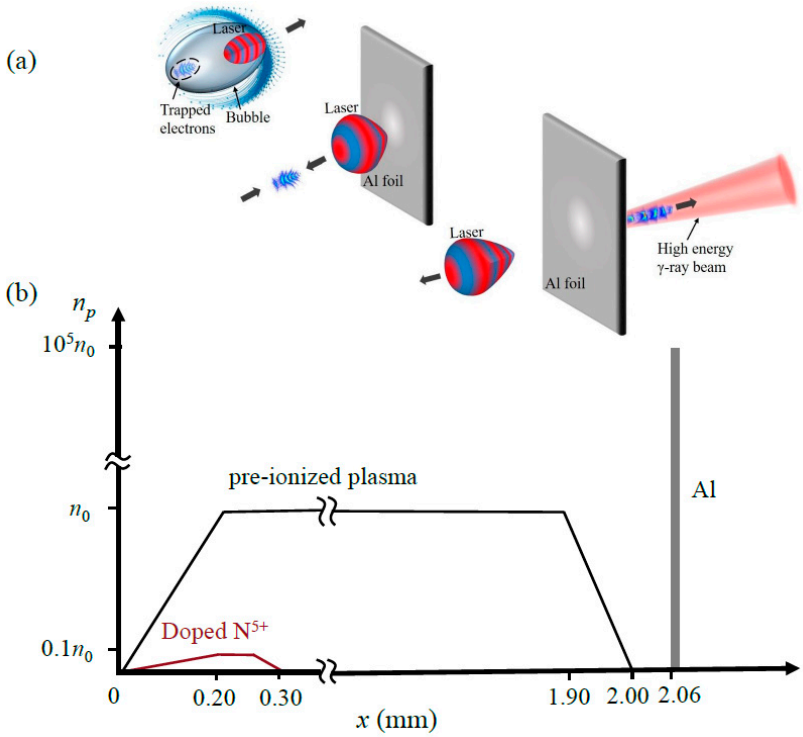

Figure 1. The schematic diagram of attosecond inverse Compton scattering source from laser wakefield acceleration. (**a**) cartoons for ICS process. Attosecond micro-bunched electron beams produced by LWFA scatter the laser pulse reflected from a fully ionized Al foil plasma. (**b**) The plasma density profiles used in the simulation setup.

Two-dimensional(2D) PIC simulations use the EPOCH open-source plasma physics simulation code [29]. A y-direction polarized laser with a Gaussian profile $a = a_0 \exp(-(t-t_0)^2/\tau^2)\exp(-y^2/w^2)$ propagates along the $+x$ direction, where $a_0 = eE_0/m_e\omega_0 c = 1.5$ is the normalized amplitude of the laser field, $2\tau\sqrt{\ln 2} = 30$ fs is the full width at half maximum (FWHM) pulse duration of the laser, and $w = w_0\sqrt{1+(x_0/x_R)^2}$. The laser is focused at $x_0 = 200$ μm with a beam waist of $w_0 = 20$ μm and $x_R = \pi w_0^2/\lambda_0$ is the Rayleigh length with $\lambda_0 = 800$ nm. A two-staged LWFA structure is proposed with a gas mixture for injection and a pure gas plasma for acceleration [30]. The doped gas mixture is set as N^{5+} ions with a concentration of $n_{N^{5+}} = 0.1n_0$. N^{5+} ions locate from $x = 0$ to $x = 300$ μm, with a 200 μm long up-ramp, and a flat of 50 μm with a 50 μm long down-ramp. Pre-ionized plasma has an electron density of $n_0 = n_{He} + 5n_{N^{5+}} = 5 \times 10^{18}$ cm^{-3} as the density profile shown in Figure 1b. The simulation window has a dimension of 40 μm $\times$ 80 μm with 2000 $\times$ 1200 cells in the x and y directions, respectively. This corresponds to the cell sizes of $0.025k_0^{-1}$ in the x direction and $0.08k_0^{-1}$ in the y direction, respectively. Each cell contains 4 macroparticles. When the laser passes through the plasma, the pre-ionized electrons (i.e., pre-ionized from

the Helium atoms and the *L*-shell of nitrogen) form the plasma wake, and electrons from the *K*-shell of nitrogen are tunneling ionized and trapped by the wake.

Downstream of the LWFA stage, a 100 μm long plasma downward density ramp (DDR) is introduced at x = 1.90 mm to guide the electron beam into the vacuum. Following this, a plasma with electron density $n_p = 10^5 n_0 \simeq 292 n_c$ is set as a fully ionized Al foil, where $n_c = 1.71 \times 10^{21} \mathrm{cm}^{-3}$ is the critical density for the laser wavelength $\lambda_0 = 800$ nm. The Al plasma is positioned at x = 2.06 mm with a thickness of 20 μm. The numbers of particles per cell for photons and Al species are set to 100. In the open-source EPOCH 2D PIC code, the nonlinear Compton scattering emission and bremsstrahlung studies used the Monte Carlo algorithm already implemented in the code [31,32]. While the driving laser pulse was effectively reflected by the plasma mirror, ICS gamma-ray photons could pass through the foil with the Bremsstrahlung radiation. In our case, the laser field is significantly weaker than the Schwinger field, so photon emission occurs in the non-QED regime [33].

3. Results and Discussion

3.1. Generation of Attosecond Micro-Bunched Electron Beams from LWFA

Nonlinear trapping in laser wakefield acceleration significantly influences the quality of the final electron beam. Ionization-induced injection [34] is favored in LWFA due to its controllability, enabling the generation of a high-brightness, stable, and tunable electron beam. According to the ionization injection dynamics [35], the relative longitudinal position $\xi \equiv x - v_\phi t$ of the trapped electron is primarily determined by the initial ξ_i as follows:

$$\xi = -\sqrt{4 + \xi_i^2 + r_i^2 - r^2 - 4[\gamma - (v_\phi/c)p_x]} \tag{2}$$

where v_ϕ is the phase velocity of the wakefield, p_x and r are the longitudinal momentum and the transverse position of the trapped electrons, and r_i and ξ_i are the initial transverse and relative longitudinal position of the trapped electrons where they are ionized, respectively. Here, parameters of positions are normalized to c/ω_p, velocities to c, and the momenta to $m_e c$, with ω_p is the plasma frequency, and m_e is the electron rest mass. In general, if $r_i, r \ll 1$ and $\gamma - (v_\phi/c)p_x \ll 1$, the longitudinal position ξ_f of trapped electron is mainly determined by the initial ξ_i, as follows:

$$\xi_f \approx -\sqrt{4 + \xi_i^2} \tag{3}$$

which means the initial modulation of ξ_i can be nonlinearly mapped to ξ_f. Due to the phase-dependent ionization within a linear polarized laser field, the initial distribution of the electrons ξ_i will have a strong modulation at $2k_0$ during the sub-cycle interaction with the laser field, where k_0 is the wavenumber of the laser pulse. As a result, a bunched beam with a periodically modulated current profile can be produced. Any spreads in r_i, r and $\gamma - (v_\phi/c)p_x$ will broaden the ξ distribution, called phase mixing during the injection. Previous simulations have shown that it is crucial to suppress phase mixing during the injection and acceleration process for maintaining the initial micro-bunched features [36].

Figure 2 shows the injection and acceleration of an attosecond pre-bunched electron beam. The snapshots of the trapped charge are shown in Figure 2a, where the injected electrons exit the gas mixture at x = 0.3 mm. It indicates that electrons are immediately micro-bunched after injection. Fine bunch structures and the on-axis density profiles show strong periodic modulation in the (ξ_f, y) space and a comb-like density bunch profile is pronounced. Figure 2b displays the initial phase space distribution (ξ_i, p_x) of the injected electrons when they are ionized in the electric field of the driving laser. Since the laser intensity is just above the ionization threshold of N^{6+}, electrons are ionized off-peak of the laser electric field and born with the initial coordinates $\xi_i < 0$, as shown in Figure 2b. Furthermore, by using a linearly polarized laser pulse, the longitudinal momentum distribution oscillates twice per laser period. Electrons ionized at different

times with the same initial ξ_i will be nonlinearly mapped to the same position ξ_f. When they are trapped by the wake, the comb-like on-axis density bunch profile is evident in Figure 2a. The average interval between the peaks of the beam density profile in Figure 2a is approximately 0.97 fs, and the average bunch length(rms) of micro bunches is about 118 as.

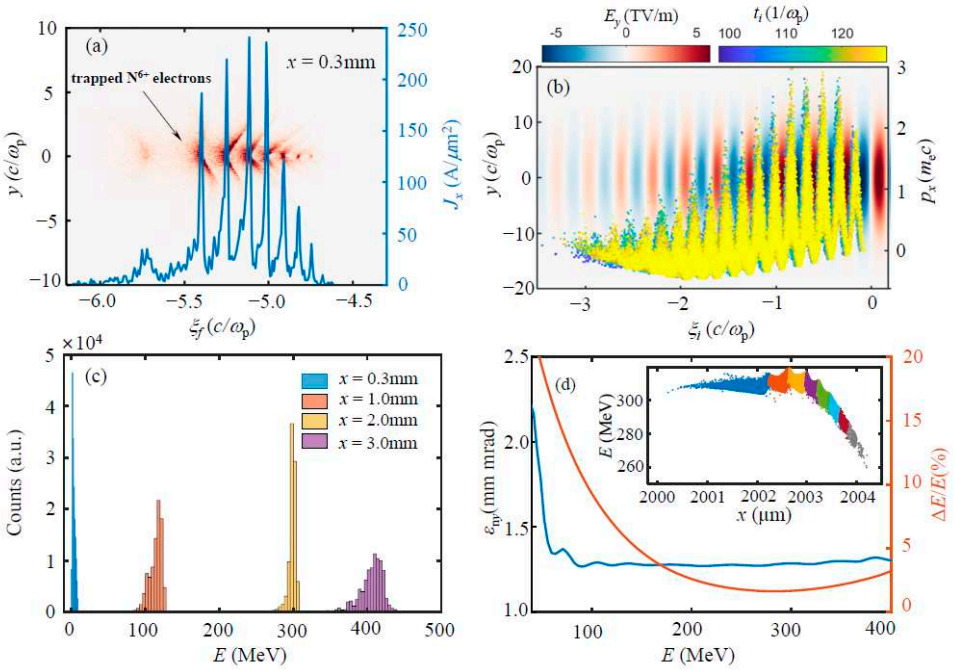

Figure 2. Dynamic evolutions of the micro-bunched electron beam in the LWFA stage. (**a**) Density distribution of the trapped nitrogen electron and the on-axis current density profile. (**b**) Initial phase space distribution of the injected electrons (ξ_i, p_x) upon ionization in the electric field E_y of the driving laser. (**c**) Energy spectra of the electron beam during 3 mm acceleration. (**d**) Normalized transverse emittance and relative energy spread evolutions of the entire beam during the acceleration, and the inset: longitudinal phase space (x, p_x) of the electron beam near x = 2 mm, where the relative energy spread of the electron beam is minimal. The individual micro bunches are highlighted in different colors.

Once the electron beam exits the gas mixture with the density-modulated structure, it continues to be accelerated. In Figure 2c, we show the energy spectra of the entire beam energy during the acceleration. Initially, the entire beam shows increasing absolute energy spread as electrons are trapped at the rear of the bubble, transitioning from the negative slope region to the positive slope of the wakefield. Electrons at the front experience a larger longitudinal accelerating field. Subsequently, in the positive slope region, electrons at the tail gain more energy than those at the front, reversing the longitudinal phase space of the electrons. As depicted in Figure 2d, at x = 2 mm, where the relative energy spread of the entire beam is at its minimum, the energy chirp of the beam will reverse, with electrons at the tail gaining more energy from the plasma wakefield before entering the deceleration phase. Furthermore, it is observed that the longitudinal phase mixing does not occur in the further acceleration to 3 mm, allowing electrons to maintain a steady phase and preserve the discrete bunching structure. The normalized transverse emittance of the entire beam is approximately 1.28 mm mrad. Additionally, the minimum relative energy spread of the micro-bunched beam is around 1.64%, with individual micro bunches (highlighted in different colors in the inset of Figure 2d) achieving even lower values.

3.2. Attosecond Gamma-Ray Source from ICS

The microbunching of the electron beam fingerprint on the ICS radiation is analyzed by applying a thin Al plasma downstream of the LWFA stage at x = 2.06 mm. Figure 3a

illustrates the evolutions of the normalized transverse emittance and relative energy spreads of the micro-bunched electron beam during the transition from LWFA to ICS process. Upon propagating into the vacuum, a head-on collision with the reflected laser pulse occurred at approximately x = 2050 μm in front of the plasma mirror, ending before the electron beam entered the Al foil plasma, where the bremsstrahlung radiation should also be considered. As shown in Figure 3a, interactions with the reflected laser field during the head-on collision result in the increased emittance and relative energy spread of the electron beam. Electrons undergo oscillations in the field of the reflected laser, as the snapshots of the electron beam at different positions (pre-collision at x = 2043 μm), during collision at x = 2053 μm), and post-collision at x = 2059 μm) depicted in Figure 3b–d. Electrons acquire additional transverse momentum during the ICS head-on collision. However, normalized emittance of the electron beam returns to 1.28 mm mrad when the head-on collision ends, with nearly zero net transverse momentum gained from the laser field throughout the process, as shown in Figure 3d. When the electrons enter the Al foil plasma, the normalized emittance increases rapidly again when the bremsstrahlung scattering occurs, as indicated by the phase spaces in Figure 3e.

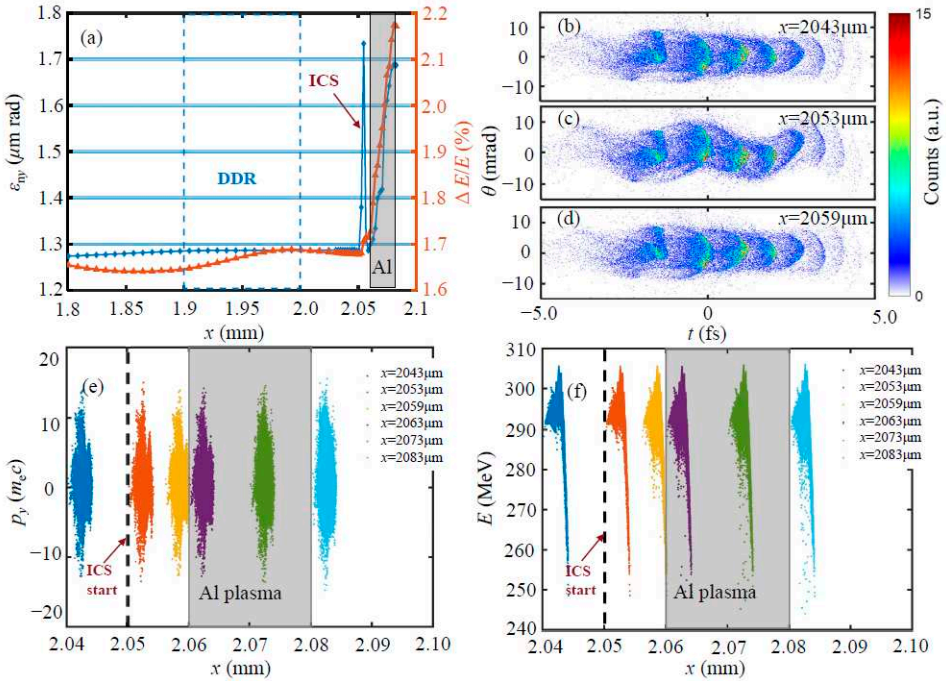

Figure 3. The dynamics of the micro bunches during the Inverse Compton scattering (ICS) process. (**a**) Evolutions of the normalized transverse emittance ε_{ny} and the relative energy spread $\Delta E/E$ of the entire beam, highlighting the DDR for the plasma density down-ramp region and gray area for the fully ionized Al plasma region. (**b**–**d**) Snapshots of the micro bunches at different times during the ICS with the reflected laser pulse. (**b**) pre-collision at x = 2043 μm, (**c**) during collision at x = 2053 μm, (**d**) post-collision at x = 2059 μm. (**e**,**f**) Electron phase space (x, p_y) and (x, E) throughout the ICS process. Dots with different colors show electrons at different positions.

Furthermore, when the micro bunches interact with the reflected driving laser pulse, the energy spread of the beam gradually increases due to the deceleration of some electrons, as depicted in the energy spectra around x = 2053 μm and x = 2059 μm shown in Figure 3f. Energy spread degradation continues further as the beam penetrates the thin plasma mirror, influenced by electron–ion collisions within the foil. Nevertheless, it can be observed that the electron beam maintains a stable micro-bunched structure throughout the ICS head-on collision, as illustrated by Figure 3b–d, both in the temporal and spatial aspects. Such micro-bunches would potentially fingerprint the inherited structure onto the gamma-ray radiation.

Figure 4a,b verifies the isolated structures with snapshots of electron and gamma-ray photon densities at the post-collision position around x = 2059 μm. The emitted photons exhibit a comb-like structure with a scale similar to that of the electron beam, as shown in Figure 4c. The single micro-pulse of the photons has an FWHM length of approximately 260 as to 300 as, with time intervals between sub-pulses ranging from 1.10 fs to 1.45 fs, which is about half of the wavelength of the driving laser and consistent with the micro bunched characteristics from LWFA. Figure 4d illustrates the spatial and temporal characteristics of the ICS radiation, which reveal a micro-sized attosecond radiation source with an rms divergence of about 4.25 mrad. The energy spectrum of photons in Figure 4e shows us a continuum spectrum. The tail of the integrated spectrum can be approximately fit by a modified Bessel function [37] as $dN/dE \sim \int_{E/E_c}^{\infty} K_{5/3}(x)dx$, with a fitted critical energy of $E_c = \hbar\omega_c \simeq 2.0 \pm 0.2$MeV.

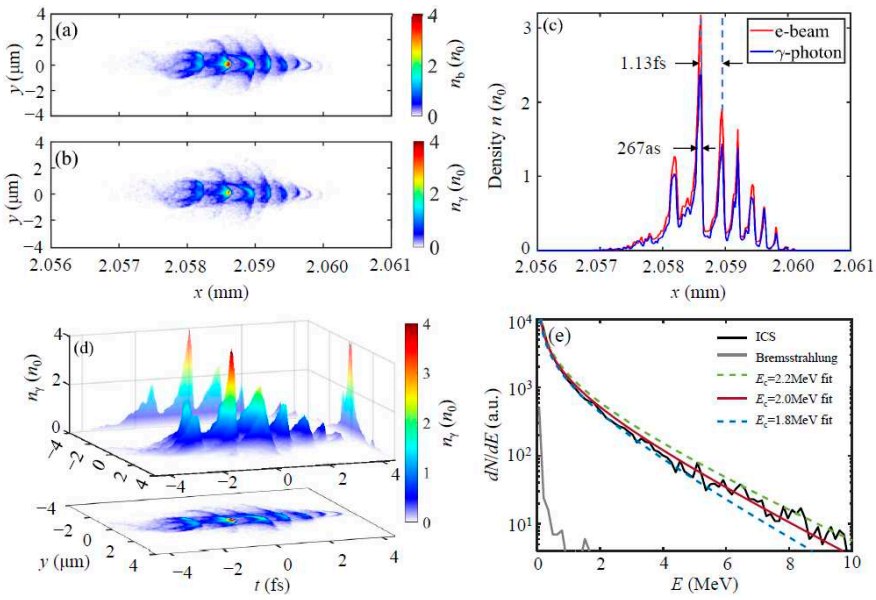

Figure 4. The temporal and spatial characteristics and energy spectrum of ICS radiation. (**a**,**b**) the density distributions of electrons and gamma photons around x = 2059 μm. (**c**) Comb-like structures on the axis density profiles for both electron beam and gamma photons. (**d**) inherit temporal and spatial distribution of the emitted gamma photons. (**e**) The energy spectrum of photons from ICS and bremsstrahlung; the critical energy of ICS is about 2.0 MeV.

Let us now proceed to estimate the peak brilliance of our source. The source size is comparable to the electron beam diameter of 2 μm at interaction, whereas the divergence of the gamma-photon beam is about 4.25 mrad. For the gamma-ray pulse with an FWHM of 267 as, as marked in Figure 4b, we have approximately 2.23×10^2 photons in a 0.1% bandwidth around 2 MeV, implying a peak brilliance of ~1.03×10^{22} photons s^{-1} mm^{-2} mrad^{-2} 0.1% BW. This brilliance is competitive with laboratory-based multi-MeV γ-ray sources using moderate-intensity laser pulses (a_0 = 1.5).

For the comparison, such electrons ($\gamma \approx 600$) oscillate in a similar plasma density of 5×10^{18} cm^{-3}, with a typical oscillation amplitude at the micrometer level. The critical energy of betatron radiation is about a few tens of keV. Additionally, the bremsstrahlung radiation spectrum shown in Figure 4e indicates emission with a cutoff energy of <2 MeV as the electrons pass through the plasma foil. In contrast, the cutoff photon energies from ICS can extend to 10 MeV. Furthermore, the total photon numbers from betatron and bremsstrahlung radiation are nearly two orders of magnitude smaller than those from the ICS gamma-ray photons.

4. Conclusions

In conclusion, we have proposed a scheme to generate an attosecond gamma-ray source by the structural fingerprints of micro bunches from LWFA. In the near-threshold ionization injection scheme, by using a linearly polarized laser at an intensity of a $a_0 = 1.5$, the phase-dependent ionization causes the injection of micro-bunched beams with dispersive comb-like longitudinal density distributions. These periodic modulations imprint onto secondary gamma-ray sources with attosecond temporal resolution upon head-on collision with the reflected laser pulse. The internal fine structures of the generated ICS source are consistent with the micro-bunches. The time intervals between sub-pulses range from 1.10 fs to 1.45 fs, which is about half of the wavelength of the driving laser, and the FWHM length of each single pulse can reach 260 as. The critical energy of the gamma-ray source is about 2 MeV, with the cut-off energy extending to 10 MeV, which yields a peak brilliance of ~10^{22} photons s^{-1} mm^{-2} $mrad^{-2}$ 0.1% BW.

Such a micro-sized attosecond gamma-ray source is expected to achieve unpredicted high brilliance with ultra-cold high-brightness electron beams by applying the plasma photocathode technique (the so-called trojan horse scheme) [38,39] under the near-threshold ionization injection. Experimentally, it is valuable to reveal the sub-micrometer structure of electron beams from plasma wakefield acceleration [40], which also critically influences gain in free-electron lasers or particle yield in colliders. Further optimization of such space–time-correlated structures of the beams and the temporal–spatial characteristics of the tabletop plasma wakefield-based X-ray sources could pave the way for new avenues in sub-femtosecond probing.

Author Contributions: Conceptualization, A.D. and Z.L.; methodology, Y.L. and Y.W.; software, Y.L., Y.W. and Z.L.; writing—original draft preparation, A.D., Y.L., Y.W. and Z.L.; writing—review and editing, A.D. and X.Y.; visualization, A.D., Y.L. and Y.W.; supervision, A.D. and J.Z. All authors have read and agreed to the published version of the manuscript.

Funding: This research was funded by the National Natural Science Foundation of China (Grant Nos. 12174343, 12005187), and the Zhejiang Provincial Natural Science Foundation of China (Grant No. LQ21A050002).

Institutional Review Board Statement: Not applicable.

Informed Consent Statement: Not applicable.

Data Availability Statement: The data presented in this study are available on request from the corresponding author. The data are not publicly available due to privacy.

Conflicts of Interest: The authors declare no conflicts of interest.

References

1. Geddes, C.G.R.; Toth, C.S.; van Tilborg, J.; Esarey, E.; Schroeder, C.B.; Bruhwiler, D.; Nieter, C.; Cary, J.; Leemans, W.P. High-quality electron beams from a laser wakefield accelerator using plasma-channel guiding. Nature. High-quality electron beams from a laser wakefield accelerator using plasma-channel guiding. *Nature* **2004**, *431*, 538–541. [CrossRef]
2. Faure, J.; Gaines, Y.; Pukhov, A.; Kiselev, S.; Gordienko, S.; Lefebvre, E.; Rousseau, J.-P.; Burgy, F.; Malka, V. A laser-plasma accelerator producing monoenergetic electron beams. *Nature* **2004**, *431*, 541–544. [CrossRef]
3. Mangles, S.P.D.; Murphy, C.D.; Najmudin, Z.; Thomas, A.G.R.; Collier, J.L.; Dangor, A.E.; Divall, E.J.; Foster, P.S.; Gallacher, J.G.; Hooker, C.J.; et al. Monoenergetic beams of relativistic electrons from intense laser-plasma interactions. *Nature* **2004**, *431*, 535–538. [CrossRef]
4. Kim, H.T.; Pathak, V.B.; Hojbota, C.I.; Mirzaie, M.; Pae, K.H.; Kim, C.M.; Yoon, J.W.; Sung, J.H.; Lee, S.K. Multi-GeV Laser Wakefield Electron Acceleration with PW Lasers. *Appl. Sci.* **2021**, *11*, 5831. [CrossRef]
5. Aniculaesei, C.; Ha, T.; Yoffe, S.; Labun, L.; Milton, S.; McCary, E.; Spinks, M.M.; Quevedo, H.J.; Labun, O.Z.; Sain, R.; et al. The acceleration of a high-charge electron bunch to 10 GeV in a 10-cm nanoparticle-assisted wakefield accelerator. *Matter Radiat. Extrem.* **2024**, *9*, 014001. [CrossRef]
6. Couperus, J.P.; Pausch, R.; Köhler, A.; Zarini, O.; Krämer, J.M.; Garten, M.; Huebl, A.; Gebhardt, R.; Helbig, U.; Bock, S.; et al. Demonstration of a beam loaded nanocoulomb-class laser wakefield accelerator. *Nat. Commun.* **2017**, *8*, 487. [CrossRef]
7. Buck, A.; Nicolai, M.; Schmid, K.; Sears, C.M.; Sävert, A.; Mikhailova, J.M.; Krausz, F.; Kaluza, M.C.; Veisz, L. Real-time observation of laser-driven electron acceleration. *Nat. Phys.* **2011**, *7*, 543–548.

8. Lundh, O.; Lim, J.; Rechatin, C.; Ammoura, L.; Ben-Ismaïl, A.; Davoine, X.; Gallot, G.; Goddet, J.P.; Lefebvre, E.; Malka, V.; et al. Few femtosecond, few kiloampere electron bunch produced by a laser–plasma accelerator. Few femtosecond, few kiloampere electron bunch produced by a laser–plasma accelerator. *Nat. Phys.* **2011**, *7*, 219–222. [CrossRef]
9. Ke, L.T.; Feng, K.; Wang, W.T.; Qin, Z.Y.; Yu, C.H.; Wu, Y.; Chen, Y.; Qi, R.; Zhang, Z.J.; Xu, Y.; et al. Near-GeV Electron Beams at a Few Per-Mille Level from a Laser Wakefield Accelerator via Density-Tailored Plasma. *Phys. Rev. Lett.* **2021**, *126*, 214801. [CrossRef]
10. Maier, A.R.; Delbos, N.M.; Eichner, T.; Hübner, L.; Jalas, S.; Jeppe, L.; Jolly, S.W.; Weingartner, M.R.; Raith, S.; Popp, A.; et al. Ultralow emittance electron beams from a laser-wakefield accelerator. *Phys. Rev. Spec. Top. Accel. Beams* **2012**, *15*, 111302.
11. Plateau, G.R.; Geddes, C.G.R.; Thorn, D.B.; Chen, M.; Benedetti, C.; Esarey, E.; Gonsalves, A.J.; Matlis, N.H.; Nakamura, K.; Schroeder, C.B.; et al. Low-emittance electron bunches from a laser-plasma accelerator measured using single-shot X-ray spectroscopy. *Phys. Rev. Lett.* **2012**, *109*, 064802. [CrossRef]
12. Corde, S.; Ta Phuoc, K.; Lambert, G.; Fitour, R.; Malka, V.; Rousse, A.; Beck, A.; Lefebvre, E. Femtosecond X-rays from laser-plasma accelerators. *Rev. Mod. Phys.* **2013**, *85*, 1–48. [CrossRef]
13. Hartmann, F.V.; Gibson, D.J.; Brown, W.J.; Rousse, A.; Phuoc, K.T.; Mallka, V.; Faure, J.; Pukhov, A.A. Compton scattering X-ray sources driven by laser wakefield acceleration. *Phys. Rev. Spec. Top. Accel. Beams* **2007**, *10*, 011310. [CrossRef]
14. Martin, M.; Hynes, J.T. *Femtochemistry and Femtobiology: Ultrafast Events in Molecular Science*; Elsevier: Oxford, UK, 2004.
15. Albert, F.; Thomas, A.G.R. Applications of laser wakefield accelerator-based light sources. *Plasma Phys. Control. Fusion* **2016**, *58*, 103001. [CrossRef]
16. Sarri, G.; Corvan, D.J.; Schumaker, W.; Cole, J.M.; Di Piazza, A.; Ahmed, H.; Harvey, C.; Keitel, C.H.; Krushelnick, K.; Mangles, S.P.D.; et al. Ultrahigh Brilliance Multi-MeV γ-Ray Beams from Nonlinear Relativistic Thomson Scattering. *Phys. Rev. Lett.* **2014**, *113*, 224801. [CrossRef]
17. Phuoc, K.T.; Corde, S.; Thaury, C.; Malka, V.; Tafzi, A.; Goddet, J.P.; Shah, R.C.; Sebban, S.; Rousse, A. All-optical Compton gamma-ray source. *Nat. Photon.* **2012**, *6*, 308. [CrossRef]
18. Powers, N.D.; Ghebregziabher, I.; Golovin, G.; Liu, C.; Chen, S.; Banerjee, S.; Umstadter, D.P. Quasi-monoenergetic and tunable X-rays from a laser-driven Compton light source. *Nat. Photonics* **2013**, *8*, 28–31. [CrossRef]
19. Chen, S.; Powers, N.D.; Ghebregziabher, I.; Maharjan, C.M.; Liu, C.; Golovin, G.; Banerjee, S.; Zhang, J.; Cunningham, N.; Moorti, A.; et al. MeV-energy X rays from inverse compton scattering with laser-wakefield accelerated electrons. *Phys. Rev. Lett.* **2013**, *110*, 155003. [CrossRef]
20. Khrennikov, K.; Wenz, J.; Buck, V.; Xu, J.; Heigoldt, M.; Veisz, L.; Karsch, S. Tunable all optical quasimonochromatic Thomson X-ray source in the nonlinear regime. *Phys. Rev. Lett.* **2015**, *114*, 195003. [CrossRef]
21. Tsai, H.-E.; Wang, X.; Shaw, J.M.; Li, Z.; Arefiev, A.V.; Zhang, X.; Zgadzaj, R.; Henderson, W.; Khudik, V.; Shvets, G.; et al. Compact tunable Compton X-ray source from laser-plasma accelerator and plasma mirror. *Phys. Plasmas* **2015**, *22*, 023106. [CrossRef]
22. Döpp, A.; Guillaume, E.; Thaury, C.; Gautier, J.; Andriyash, I.; Lifschitz, A.; Malka, V.; Rousse, A.; Phuoc, K.T. An all-optical Compton source for single-exposure X-ray imaging. *Plasma Phys. Control. Fusion* **2016**, *58*, 034005. [CrossRef]
23. Yu, C.; Qi, R.; Wang, W.; Liu, J.; Li, W.; Wang, C.; Zhang, Z.; Liu, J.; Qin, Z.; Fang, M.; et al. Ultrahigh brilliance quasi-monochromatic MeV gamma-rays based on self-synchronized all-optical Compton scattering. *Sci. Rep.* **2016**, *6*, 29518.
24. Hannasch, A.; Garcia, A.L.; LaBerge, M.; Zgadzaj, R.; Köhler, A.; Couperus Cabadağ, J.P.; Zarini, O.; Kurz, T.; Ferrari, A.; Molodtsova, M.; et al. Compact spectroscopy of keV to MeV X-rays from a laser wakefield accelerator. *Sci. Rep.* **2021**, *11*, 14368. [CrossRef]
25. Krämer, J.M.; Jochmann, A.; Budde, M.; Bussmann, M.; Couperus, J.P.; Cowan, T.E.; Debus, A.; Köhler, A.; Kuntzsch, M.; García, A.L.; et al. Making spectral shape measurements in in-verse Compton scattering a tool for advanced diagnostic applications. *Sci. Rep.* **2018**, *8*, 1398. [CrossRef]
26. Brümmer, T.; Bohlen, S.; Grüner, F.; Osterhoff, J.; Põder, K. Compact all-optical precision-tunable narrowband hard Compton X-ray source. *Sci. Rep.* **2022**, *12*, 16017. [CrossRef]
27. Maroju, P.K.; Grazioli, C.; Fraia, M.; Moioli, M.; Ertel, D.; Ahmadi, H.; Plekan, O.; Finetti, P.; Allaria, E.; Giannessi, L.; et al. Attosecond pulse shaping using a seeded free-electron laser. *Nature* **2020**, *578*, 386–391. [CrossRef]
28. Duris, J.P.; MacArthur, J.P.; Glownia, J.M.; Li, S.; Vetter, S.; Miahnahri, A.; Coffee, R.; Hering, P.; Fry, A.; Welch, M.E.; et al. Controllable X-ray pulse trains from enhanced self-amplified spontaneous emission. *Phys. Rev. Lett.* **2021**, *126*, 104802. [CrossRef] [PubMed]
29. Arber, T.D.; Bennett, K.; Brady, C.S.; Lawrence-Douglas, A.; Ramsay, M.G.; Sircombe, N.J.; Gillies, P.; Evans, R.G.; Schmitz, H.; Bell, A.R.; et al. Contemporary particle-in-cell approach to laser-plasma modeling. *Plasma Phys. Control. Fusion* **2015**, *57*, 113001. [CrossRef]
30. Mirzaie, M.; Li, S.; Zeng, M.; Hafz, N.A.M.; Chen, M.; Li, G.Y.; Zhu, Q.J.; Liao, H.; Sokollik, T.; Liu, F.; et al. Demonstration of self-truncated ionization injection for GeV electron beams. *Sci. Rep.* **2015**, *5*, 14659. [CrossRef]
31. Ridgers, C.; Kirk, J.; Duclous, R.; Blackburn, T.; Brady, C.; Bennett, K.; Arber, T.; Bell, A. Modelling gamma-ray photon emission and pair production in high-intensity laser–matter interactions. *J. Comput. Phys.* **2014**, *260*, 273–285. [CrossRef]
32. Morris, S.; Robinson, A.; Ridgers, C.P. Highly efficient conversion of laser energy to hard X-rays in high-intensity laser–solid simulations. *Phys. Plasmas* **2021**, *28*, 103304. [CrossRef]

33. Qiao, B.; Chang, H.X.; Xie, Y.; Xu, Z.; He, X.T. Gamma-ray generation from laser-driven electron resonant acceleration: In the non-QED and the QED regimes. *Phys. Plasmas* **2017**, *24*, 123101. [CrossRef]
34. Pak, A.; Marsh, K.A.; Martins, S.F.; Lu, W.; Mori, W.B.; Joshi, C. Injection and trapping of tunnel-ionized electrons into laser-produced wakes. *Phys. Rev. Lett.* **2010**, *104*, 025003. [CrossRef] [PubMed]
35. Xu, X.L.; Pai, C.H.; Zhang, C.J.; Li, F.; Wan, Y.; Wu, Y.P.; Hua, J.F.; Lu, W.; An, W.; Yu, P.; et al. Nanoscale electron bunching in laser-triggered ionization injection in plasma accelerators. *Phys. Rev. Lett.* **2016**, *117*, 034801. [CrossRef] [PubMed]
36. Deng, A.; Li, X.; Luo, L.; Li, Y.; Zeng, J. Generation of attosecond micro bunched beam using ionization injection in laser wakefield acceleration. *Opt. Express* **2023**, *31*, 19958–19967. [CrossRef]
37. Li, M.; Chen, L.; Li, D.; Huang, K.; Li, Y.; Ma, Y.; Yan, W.; Tao, M.; Tan, J.; Sheng, Z.; et al. Collimated gamma rays from laser wakefield accelerated electrons. *Matter Radiat. Extrem.* **2018**, *3*, 188–196. [CrossRef]
38. Hidding, B.; Pretzler, G.; Rosenzweig, J.B.; Königstein, T.; Schiller, D.; Bruhwiler, D.L. Ultracold Electron Bunch Generation via Plasma Photocathode Emission and Acceleration in a Beam-Driven Plasma Blowout. *Phys. Rev. Lett.* **2012**, *108*, 035001. [CrossRef]
39. Deng, A.; Karger, O.S.; Heinemann, T.; Knetsch, A.; Scherkl, P.; Manahan, G.G.; Beaton, A.; Ullmann, D.; Wittig, G.; Habib, A.F.; et al. Generation and acceleration of electron bunches from a plasma photocathode. *Nat. Phys.* **2019**, *15*, 1156–1160. [CrossRef]
40. LaBerge, M.; Bowers, B.; Chang, Y.Y.; Cabadağ, J.C.; Debus, A.; Hannasch, A.; Pausch, R.; Schöbel, S.; Tiebel, J.; Ufer, P.; et al. Revealing the three-dimensional structure of microbunched plasma-wakefield-accelerated electron beams. *Nat. Photonics* **2024**. [CrossRef]